Coherent propagation of Stokes light in a collisionally broadened three-level amplifier

B. J. Herman* and J. H. Eberly†
Department of Physics and Astronomy, University of Rochester, Rochester, New York 14627

M. G. Raymer‡
Institute of Optics, University of Rochester, Rochester, New York 14627
(Received 24 August 1988)

We undertake a theoretical investigation of the coherent optical propagation of Stokes light in a collisionally broadened three-level Raman amplifier. The Stokes light consists of two distinct spectral components: off-resonance stimulated Raman scattering and on-resonance stimulated fluorescence, induced by collisional transfer of population to a near-resonant intermediate state of the atomic system. Our model is based on the semiclassical Maxwell-Bloch formalism where the separation of the Stokes light into two components results in an expansion from the usual 9 to 13 atomic variables. We investigate the model both analytically and numerically. We point out the physical contributions to the simultaneous evolution of pump, fluorescence, and Raman light. We discuss the development during propagation of these separate pulses, emphasizing the nonlinear effects that lead to saturation.

I. INTRODUCTION

The model of two radiation fields interacting with a three-level system is central to many problems in quantum optics which deal with pulse propagation, including solitons,[1,2] stimulated Raman scattering (SRS),[3–5] superfluorescence,[6,7] and parametric amplification.[8] In an amplifier configuration [Fig. 1(a)], the atoms are pumped on the first transition ($1\leftrightarrow2$) by irradiation with a laser pulse. Light scattered to the second transition ($2\leftrightarrow3$) can be amplified through the process of stimulated emission. The frequency of the amplified light depends upon the pump-laser frequency. Two types of output light are possible: fluorescence, when the laser is tuned on resonance with the pumping transition and the light is emitted at the resonance frequency of the amplifying transition [Fig. 1(b)], and Raman scattering, when the pump is tuned off resonance and the light is scattered from a laser-induced virtual level [Fig. 1(c)]. Both types of light are generally referred to as Stokes light.

In the usual theoretical treatment of Raman scattering,[3–5] the pump laser is assumed to be tuned far off resonance from any higher-lying intermediate state which provides the dipole coupling that allows the Raman scattering. It is clear, however, that as the pump is tuned closer to the intermediate state there will come a point when thermal energies, due to collisions between atoms, can impart additional kinetic energy to take population from the virtual level to the upper state [Fig. 1(d)].[9–17] The atom then can decay, producing fluorescence. If the collisional broadening is strong enough, this mechanism can occur even when the laser is tuned well outside of the natural linewidth of the pump transition. This leads to a possibility of *simultaneous* growth of fluorescence and Raman light in a collisionally broadened amplifier. In this paper we develop a theory to account for the propagation of Stokes light in this type of medium. We will be particularly concerned with nonlinear effects which lead to saturation and competition between the different components of the Stokes light.

Distinct Raman and fluorescence components occurring simultaneously on the same transition have been seen in experiments. Wynne and Sorokin[10] observed separate spectral components and their interaction when tuning near a resonance line in potassium vapor. Competition between components has been proposed as a possible explanation of results seen in some early attempts by Carlsten and Dunn[11] to generate tunable radiation through stimulated Raman scattering by near-resonance pumping with a dye laser. In these experiments, as resonance was approached, SRS output was seen to decrease instead of exhibiting an expected increase.

The situation was somewhat clarified by Raymer and Carlsten,[13–16] who observed the simultaneous amplification of both Raman and fluorescence light in ex-

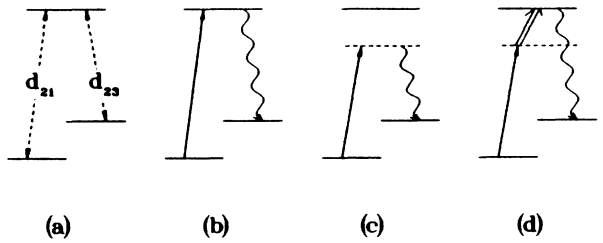

FIG. 1. (a) Level configuration of the three-level amplifier. The dashed lines show the allowed dipole couplings. (b) Generation of fluorescence in the amplifying transition by on-resonance tuning in the pump transition. (c) Generation of Raman scattering in the amplifying transition by off-resonance tuning in the pump transition. (d) Generation of collision-induced fluorescence by collisional population transfer (double arrow) from laser-induced virtual level to upper state.

periments on atomic thallium in an argon buffer gas. The growth from spontaneous to stimulated emission in both types of light was discussed by them using gain theories. Their treatment, however, ignored population depletion and coherence effects and thus could not explain the saturation behavior observed in their experiments.

The collision process takes energy away from the pump pulse, which otherwise would have gone into Raman scattering, and makes it available for fluorescence. It is important to understand how the output pulses compete for energy from the pump pulse since it will affect the Raman conversion process. It is also of interest to investigate the development of the fluorescence and Raman light since they exhibit different spatial and temporal behavior due to the different physical mechanisms which produce them. It is well known that fluorescence exhibits a lifetime independent of the pump pulse, while Raman scattering is only generated while the pump pulse is turned on.[12,18]

In Sec. II we derive the equations of motion which serve as the basis of our model. Analytic results for several limits of these equations are discussed in Sec. III. In Sec. IV we discuss our numerical results, paying particular attention to nonlinear effects. We treat inhomogeneous broadening effects in Sec. V. In Sec. VI we summarize our results.

II. EQUATIONS OF MOTION

A. Optical Bloch equations

We choose to work in the Heisenberg picture and treat the atom-field interaction semiclassically. We take as our model the three-level atom shown in Fig. 2. The ground, intermediate, and excited states are labeled as $|1\rangle$, $|2\rangle$, and $|3\rangle$, respectively. Dipole transitions are allowed between levels 1 and 2 and 2 and 3 but forbidden between 1 and 3. The 1-2 transition is pumped off resonance by a field $\mathbf{E}_P$ and the 2-3 transition is probed by $\mathbf{E}_S$. We take the total electric field to have the form

$$\mathbf{E}(z,t)=\mathbf{E}_P(z,t)+\mathbf{E}_S(z,t) , \tag{2.1}$$

where

$$\mathbf{E}_P(z,t)=\mathbf{e}_P\mathcal{E}_P(z,t)\exp[-i(\omega_P t-k_P z)]+\text{c.c.} , \tag{2.2a}$$

$$\mathbf{E}_S(z,t)=\mathbf{e}_S\mathcal{E}_S(z,t)\exp[-i(\omega_S t-k_S z)]+\text{c.c.} \tag{2.2b}$$

Here, $k_a=\omega_a/c$, $\mathcal{E}_a(z,t)$ is the electric field envelope with carrier frequency ω_a, taken to vary slowly in an optical cycle, and $\mathbf{e}_a$ is its corresponding polarization vector. The carrier frequencies for the pump and Stokes waves are denoted by ω_P and ω_S, respectively, and c is the speed of light.

The atomic dynamics can be found by solving for the behavior of the atomic projection operators, $\hat{\sigma}_{jk}=|j\rangle\langle k|$, using the Heisenberg equations of motion in the dipole approximation. We will work with equations for the averages of the atomic operators by taking quantum expectation values, which we will denote by $\sigma_{jk}=\langle\hat{\sigma}_{jk}\rangle$. The expectation values of the off-diagonal atomic projection operators describe the atomic coherences in the system. As they are driven by the electric field, we will represent them by slowly varying amplitudes with appropriate oscillatory factors. We use the notation

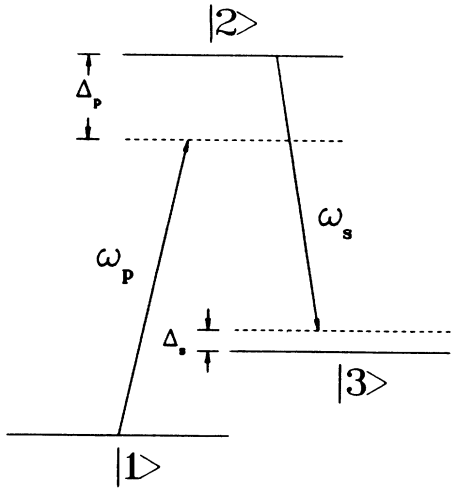

FIG. 2. Model three-level atom. 1-2 transition is pumped at frequency $\omega_P=\omega_{21}-\Delta_P$. 2-3 transition is probed at frequency $\omega_S=\omega_{23}-\Delta_S$.

$$\sigma_{jj}=s_{jj} , \tag{2.3a}$$

$$\sigma_{21}=s_{21}\exp[i(\omega_P t-k_P z)] , \tag{2.3b}$$

$$\sigma_{32}=s_{32}\exp[-i(\omega_S t-k_S z)] , \tag{2.3c}$$

$$\sigma_{31}=s_{31}\exp\{-i[(\omega_S-\omega_P)t-(k_S-k_P)z]\} , \tag{2.3d}$$

and employ the rotating-wave approximation. The resulting equations are the three-level optical Bloch equations[1,19] (OBE) and are given in Appendix A.

To account for the different output frequencies of the amplifier, we now assume that the Stokes field can be written as the sum of two distinct oscillatory components, one at the fluorescence and the other at the Raman frequency:[20]

$$\begin{aligned}\mathbf{E}_S&=\mathbf{E}_F+\mathbf{E}_R\\&=\mathbf{e}_F\mathcal{E}_F\exp[-i(\omega_F t-k_F z)]\\&\quad+\mathbf{e}_R\mathcal{E}_R\exp[-i(\omega_R t-k_R z)]+\text{c.c.}\end{aligned} \tag{2.4}$$

Here, $\omega_F=\omega_S$ and $\omega_R=\omega_F-\Delta_P^0$, where Δ_P^0 is the detuning of the pump pulse from the stationary atom [see Appendix A, Eq. (A10)]. The separation of the Stokes field into two parts suggests that we must also separate the coherences which are driven by the Stokes field into similar components:

$$s_{32}=f_{32}+r_{32}\exp[i\Delta_P^0(t-z/c)] , \tag{2.5a}$$

$$s_{31}=f_{31}+r_{31}\exp[i\Delta_P^0(t-z/c)] . \tag{2.5b}$$

By using the adiabatic approximation,[21] which allows us to assume that the field envelopes do not vary appreciably in a time $1/\Delta_P^0$, we can obtain separate equations for f_{32},

f_{31}, r_{32}, and r_{31} by inserting the ansatz (2.5) into the OBE [Eqs. (A4e) and (A4f) in Appendix A]. For the s_{32} coherence we find

$$\frac{\partial}{\partial t}f_{32}=-(\beta_{32}+i\Delta_S)f_{32} -\frac{i}{2}[\Omega_F(s_{22}-s_{33})-\Omega_P f_{31}] , \tag{2.6a}$$

$$\frac{\partial}{\partial t}r_{32}=-[\beta_{32}+i(\Delta_S+\Delta_P^0)]r_{32} -\frac{i}{2}[\Omega_R(s_{22}-s_{33})-\Omega_P r_{31}] , \tag{2.6b}$$

where the Rabi frequencies are defined as

$$\Omega_P\equiv\frac{2}{\hbar}\mathbf{d}_{21}\cdot\mathbf{e}_P\mathcal{E}_P , \tag{2.7a}$$

$$\Omega_R\equiv\frac{2}{\hbar}\mathbf{d}_{23}\cdot\mathbf{e}_R\mathcal{E}_R , \tag{2.7b}$$

$$\Omega_F\equiv\frac{2}{\hbar}\mathbf{d}_{23}\cdot\mathbf{e}_F\mathcal{E}_F , \tag{2.7c}$$

and $\mathbf{d}_{jk}=\langle j|\hat{\mathbf{d}}|k\rangle$ is a matrix element of the dipole moment operator, $\hat{\mathbf{d}}$. The detuning Δ_S and the damping constant β_{32} are given below [Eqs. (2.9b) and (2.10b)]. A similar result is found for s_{31}.

Equation (2.6b) is identical in form to Eq. (2.6a), as can be seen by setting $R\rightarrow F$, except for the additional detuning, Δ_P^0. That is, f_{32} is driven on resonance, while r_{32} is driven off resonance. Since the dipoles are proportional to the coherences, we see that we can identify f_{32} with the fluorescence part of the 2-3 dipole and r_{32} with the Raman part.

The adiabatic approximation can further be used to reduce the atomic equations by letting the coherences which are driven off resonance (s_{21}, f_{31}, r_{32}) be represented by their slowly varying residues, obtained by setting

$$\partial s_{21}/\partial t=\partial f_{31}/\partial t=\partial r_{32}/\partial t=0 .$$

This gives us our final reduced set of atomic equations:

$$\frac{\partial}{\partial t}s_{11}=\frac{i}{2}(\Omega_P^* s_{12}-\text{c.c.})+A_{21}s_{22} , \tag{2.8a}$$

$$\frac{\partial}{\partial t}s_{22}=\frac{i}{2}(\Omega_P s_{21}+\Omega_R r_{23}+\Omega_F f_{23}-\text{c.c.})-(A_{21}+A_{23})s_{22} , \tag{2.8b}$$

$$\frac{\partial}{\partial t}s_{33}=\frac{i}{2}(\Omega_R^* r_{32}+\Omega_F^* f_{32}-\text{c.c.})+A_{23}s_{22} , \tag{2.8c}$$

$$\frac{\partial}{\partial t}r_{31}=-[\beta_{31}+i(\Delta_S-\Delta_P+\Delta_P^0)]r_{31}-\frac{i}{2}(\Omega_R s_{21}-\Omega_P^* r_{32}) , \tag{2.8d}$$

$$\frac{\partial}{\partial t}f_{32}=-(\beta_{32}+i\Delta_S)f_{32}-\frac{i}{2}[\Omega_F(s_{22}-s_{33})-\Omega_P f_{31}] , \tag{2.8e}$$

where s_{21}, r_{32}, and f_{31} are understood to be replaced by their adiabatic solutions:

$$s_{21}=-\frac{i}{2}\frac{\left[\Omega_P^*(s_{11}-s_{22})+\Omega_R^* r_{31}+\frac{i}{2}\frac{\Omega_F^*\Omega_P^* f_{32}}{\beta_{21}+i(\Delta_S-\Delta_P)}\right]}{(\beta_{21}-i\Delta_P)+\frac{|\Omega_F|^2}{4[\beta_{31}+i(\Delta_S-\Delta_P)]}} \tag{2.8f}$$

$$r_{32}=-\frac{1}{\beta_{32}+i(\Delta_S+\Delta_P^0)}\frac{i}{2}[\Omega_R(s_{22}-s_{33})-\Omega_P r_{31}] , \tag{2.8g}$$

$$f_{31}=-\frac{1}{\beta_{31}+i(\Delta_S-\Delta_P)}\frac{i}{2}(\Omega_F s_{21}-\Omega_P^* f_{32}) . \tag{2.8h}$$

The detunings are defined by

$$\Delta_P\equiv\omega_{21}-\omega_P , \tag{2.9a}$$

$$\Delta_S\equiv\omega_{23}-\omega_S . \tag{2.9b}$$

We have introduced phenomenological constants to account for the damping in the system.[22] Spontaneous decay from level $|j\rangle$ to level $|k\rangle$ is described by the Einstein decay rate A_{jk}, and the dipole dephasing rates β_{jk} are made up of natural line broadening and collisional dephasing rates, γ_{jk}:

$$\beta_{21}=\tfrac{1}{2}(A_{21}+A_{23})+\gamma_{21} , \tag{2.10a}$$

$$\beta_{32}=\tfrac{1}{2}(A_{21}+A_{23})+\gamma_{32} , \tag{2.10b}$$

$$\beta_{31}=\gamma_{31} , \tag{2.10c}$$

and $\beta_{jk}=\beta_{kj}$.

B. Maxwell's equation

Under the usual slowly-varying-envelope approximation,[19] and assuming all fields are copropagating, the one-dimensional Maxwell equation that describes plane-wave propagation reduces to three separate equations, which we write in terms of the Rabi frequencies:

$$\left[\frac{\partial}{\partial z}+\frac{1}{c}\frac{\partial}{\partial t}\right]\Omega_P=2i\kappa_P\langle s_{12}\rangle_{\Delta_{21}}\ , \tag{2.11a}$$

$$\left[\frac{\partial}{\partial z}+\frac{1}{c}\frac{\partial}{\partial t}\right]\Omega_F=2i\kappa_F\langle f_{32}\rangle_{\Delta_{23}}\ , \tag{2.11b}$$

$$\left[\frac{\partial}{\partial z}+\frac{1}{c}\frac{\partial}{\partial t}\right]\Omega_R=2i\kappa_R\langle r_{32}\rangle_{\Delta_{23}}\ , \tag{2.11c}$$

where we define coupling coefficients

$$\kappa_P=\frac{N|\mathbf{d}_{21}\cdot\mathbf{e}_P|^2\omega_P}{2\epsilon\hbar c}\ , \tag{2.12a}$$

$$\kappa_F=\frac{N|\mathbf{d}_{23}\cdot\mathbf{e}_F|^2\omega_F}{2\epsilon\hbar c}\ , \tag{2.12b}$$

$$\kappa_R=\frac{N|\mathbf{d}_{23}\cdot\mathbf{e}_R|^2\omega_R}{2\epsilon\hbar c}\ . \tag{2.12c}$$

Here, N is the (uniform) number density of atoms per unit volume, ϵ is the electric permittivity of the medium, and $\langle\ \rangle_{\Delta_{jk}}$ denotes a Doppler averaging on the j-k transition performed over detunings instead of velocities. The derivation of these equations is sketched in Appendix A.

Equations (2.8) and (2.11) form the basis for our analytical and numerical investigations. It should be noted that the separation of Stokes components has led to an increased complexity in the three-level OBE. Instead of the 9 atomic variables in Eqs. (A4) there are now 13. There is also an additional electric field. The complexity is somewhat alleviated by use of the adiabatic elimination. The remaining coherences that are driven on resonance (f_{32} and r_{31}) are responsible for the major contributions to the fluorescence and Raman dipoles. The main benefit of this approach is that the field amplitudes $\mathcal{E}_F$ and $\mathcal{E}_R$ are slowly varying, in contrast to $\mathbf{E}_S$.

III. ANALYTIC RESULTS

We propose to analyze Eqs. (2.8) and (2.11) in several limits by reducing the complexity of the full set of atomic equations. This will help us to understand differences between the separate spatial and temporal developments of the Stokes components during propagation. Interactions between the Stokes components are mediated through the 2-3 inversion. Retention of these terms are in the equations makes analytic solutions intractable. These effects will be treated numerically in Sec. IV.

Before we begin, we will simplify the mathematical description of our equations by making a coordinate transformation to the moving frame. The transformation is described by the relations

$$z'=z,\quad \tau=t-z/c\ . \tag{3.1}$$

This implies a change in the derivative terms in the OBE and Maxwell equations, given by

$$\frac{\partial}{\partial t}\rightarrow\frac{\partial}{\partial\tau},\quad \frac{\partial}{\partial z}+\frac{1}{c}\frac{\partial}{\partial t}\rightarrow\frac{\partial}{\partial z'}\ . \tag{3.2}$$

z' remains the propagation distance while τ becomes the retarded time. Henceforth we will drop the prime on z'.

We will also make some simplifying assumptions for all of our analytic limits.

(1) We ignore Doppler broadening and set $\Delta_S^0=0$. This implies that we take

$$\Delta_P=\Delta_P^0,\quad \Delta_S=0\ . \tag{3.3}$$

(2) We take the Stokes components to be well separated in the output spectrum. This requires that the pump detuning be much larger than the dephasing rates:

$$|\Delta_P|\gg\beta_{jk}\ . \tag{3.4}$$

(3) We recognize that the adiabatic approximation restricts us to the weak-field limit

$$|\Omega_P|\ll|\Delta_P|\ . \tag{3.5}$$

In each of the subsections below, we will make additional assumptions for particular analytic limits.

A. Steady-state gains

Insight into the physical processes which contribute to amplification can be gained by examining Eqs. (2.8) and (2.11) in their simplest limit, that of rate equations. Rate equations have been used extensively to determine steady-state gain coefficients. Steady-state treatments of SRS are well known.[4] The first explicit treatment of steady-state growth of collision-induced fluorescence was given by Mollow.[23] Courtens and Szöke[12] and later Raymer and Carlsten[13–16] employed the dressed-state formalism to obtain gain coefficients for both fluorescence and Raman scattering. Our results reduce to their expressions in certain limits, which we discuss below.

The simple exponential growth associated with gain coefficients can be obtained from our equations under the following additional assumptions.

(1) The pump pulse is undepleted during propagation. To ensure this, we will assume

$$s_{11}(z,\tau)\simeq 1\ . \tag{3.6}$$

(2) The population in levels 2 and 3 is independent of propagation distance. This implies that population transfer between these levels occurs only through spontaneous emission and is independent of the Stokes field. Consequently, we require

$$|\Omega_F|,|\Omega_R|\ll|\Omega_P|\ . \tag{3.7}$$

This assumption will only be true for short propagation distances as exponential gain will quickly amplify the Stokes components to levels where they can modify the population distribution in the atoms.

Steady-state response of the coherences (and thus the dipoles) occurs when the collisional damping rates are much larger than other rates which appear in the atomic dynamics. The steady-state values are obtained by setting $\partial f_{32}/\partial\tau=\partial r_{31}/\partial\tau=0$. We find

$$f_{32}=-\frac{i}{2}\frac{1}{\beta_{32}}\left[(s_{22}-s_{33})-\frac{1}{4}\frac{|\Omega_P|^2}{\Delta_P^2}\right]\Omega_F\ , \tag{3.8a}$$

$$r_{31}=-\frac{1}{4}\frac{1}{\beta_{31}}\frac{\Omega_P^*\Omega_R}{\beta_{21}-i\Delta_P}\ , \tag{3.8b}$$

where we have ignored terms contributing to the ac Stark shifts.

Using these results in the Maxwell equations shows that the fields evolve exponentially. We write the results in terms of the field intensities, defined as

$$I_P=2\epsilon c|\mathcal{E}_P|^2=\frac{\epsilon c\hbar^2}{2|\mathbf{d}_{21}\cdot e_P|^2}|\Omega_P|^2\ , \tag{3.9}$$

etc. Then

$$I_P(z,\tau)=I_P(z=0,\tau)\exp(-g_Pz)\ , \tag{3.10a}$$

$$I_F(z,\tau)=I_F(z=0,\tau)\exp(g_Fz)\ , \tag{3.10b}$$

$$I_R(z,\tau)=I_R(z=0,\tau)\exp(g_Rz)\ , \tag{3.10c}$$

where the gain coefficients are given by

$$g_P=2\kappa_P\frac{\beta_{21}}{\Delta_P^2}\ , \tag{3.11a}$$

$$g_F=2\kappa_F\frac{1}{\beta_{32}}\left[(s_{22}-s_{33})-\frac{1}{4}\frac{|\Omega_P|^2}{\Delta_P^2}\right]\ , \tag{3.11b}$$

$$g_R=2\kappa_R\frac{1}{\Delta_P^2}\left[\beta_{32}(s_{22}-s_{33})+\frac{1}{4}\frac{|\Omega_P|^2}{\beta_{31}}\right]\ . \tag{3.11c}$$

The assumption of nondepletion of the pump restricts us to values $g_Pz\ll 1$.

The simple description of experimental gains allows us to determine how fast the fluorescence and Raman pulses grow with respect to each other by comparing the gain coefficients. First, however, we will look at the individual terms in the expressions (3.11b) and (3.11c).

Two terms contribute to the fluorescence. The first, proportional to the 2-3 inversion, serves as a source for fluorescence when it is positive. A positive inversion is created by the collisional transfer of population to the upper state. The second term, proportional to $-\frac{1}{4}|\Omega_P|^2/\Delta_P^2$, corresponds to a weaker two-photon process. Since it is negative, it is an absorptive process. Physically, this term describes a scattering consisting of the emission of a pump photon combined with the simultaneous absorption of a fluorescence photon. Although this term will be seen to be negligible in the rate-equation limit, it must be included in a more general discussion because initially it is the only term to make a contribution to fluorescence since the atoms start in the ground state.

The importance of collisions to the amplification of fluorescence can be seen from the s_{22} population equation. The maximum amount of population that can be transferred to the upper state is obtained by setting $\partial s_{22}/\partial\tau=0$ in Eq. (2.8b). We find

$$\begin{aligned}s_{22_{\max}}&=\frac{1}{2}\frac{\beta_{21}}{A_{21}+A_{23}}\frac{|\Omega_P|^2}{\Delta_P^2}\\&=\frac{1}{2}\frac{\gamma_{21}}{A_{21}+A_{23}}\frac{|\Omega_P|^2}{\Delta_P^2}+\frac{1}{4}\frac{|\Omega_P|^2}{\Delta_P^2}\ ,\end{aligned} \tag{3.12}$$

where we have used Eq. (2.10a). But the second term on the right-hand side of Eq. (3.12) is exactly canceled by the absorptive two-photon term

$$s_{22_{\max}}-\frac{1}{4}\frac{|\Omega_P|^2}{\Delta_P^2}=\frac{1}{2}\frac{\gamma_{21}}{A_{21}+A_{23}}\frac{|\Omega_P|^2}{\Delta_P^2}\ . \tag{3.13}$$

Since s_{22} is the only term to make a positive contribution to the gain, this shows that *in the absence of collisions ($\gamma_{21}=0$), the fluorescence cannot grow.* This result has been discussed previously by various authors.[16,24] The statement is a general one and does not apply only to the rate-equation limit.

The situation is actually somewhat more complicated than this because, while the upper state is being excited, spontaneous decays populate level 3. Thus the collisional broadening must be larger than a certain threshold amount to obtain a positive gain. We can get an estimate of the 2-3 inversion by assuming a square pump pulse and integrating Eqs. (2.8b) and (2.8c). We find

$$s_{22}-s_{33}=\tfrac{1}{2}\beta_{21}\frac{|\Omega_P|^2}{\Delta_P^2}\frac{1}{(A_{21}+A_{23})^2}((A_{21}+2A_{23})\{1-\exp[-(A_{21}+A_{23})\tau]\}-A_{23}(A_{21}+A_{23})\tau),\quad 0\le\tau\le\tau_P \tag{3.14}$$

with τ_P the pump pulse width. The condition for positive gain can be found from the expression for maximum gain, obtained by setting $\partial g_F/\partial\tau=0$ in Eq. (3.11b) and using Eq. (3.14). We find we must have

$$\gamma_{21}>\frac{1}{2}\frac{A_{21}(A_{21}+A_{23})\ln\left[2+\dfrac{A_{21}}{A_{23}}\right]}{A_{21}+A_{23}\left[1-\ln\left[2+\dfrac{A_{21}}{A_{23}}\right]\right]} \tag{3.15}$$

in order that g_F be positive.

We point out that these results are strictly true only for a constant pump pulse. It is evident that growth of the fluorescence can also occur after the pump is turned off through spontaneous decay of the upper state.

In the rate-equation limit we are concerned with large collision rates, so we will assume for the moment that (3.15) is well satisfied. Then the inversion term in the fluorescence gain will be much larger than the absorptive term. Taking the collision term to be dominant allows us to simplify the gain coefficient to

$$g_F\simeq 2\kappa_F\frac{1}{\beta_{32}}(s_{22}-s_{33})\ . \tag{3.16}$$

Previous treatments of collision-induced fluores-

cence[13–16,23] have obtained this result except that the time-dependent inversion was replaced by a "quasi"-steady-state value. This value occurs for times such that $A_{21} \gg 1/\tau \gg A_{23}$. Essentially this means that the solution is valid for times when the upper-state population has reached a steady state and there is no significant decay to level 3. This result is obtained in our equations by substituting the maximum contribution to fluorescence, Eq. (3.13), for the inversion in Eq. (3.16):

$$g_F^{(\mathrm{QSS})} = \kappa_F \frac{\gamma_{21}}{\beta_{32}(A_{21}+A_{23})} \frac{|\Omega_P|^2}{\Delta_P^2} . \tag{3.17}$$

It is clear that the quasi-steady-state solution is very restrictive as it requires the assumption that the spontaneous decays vary by orders of magnitude. It also ignores the essential fact that the fluorescence gain is *time-dependent.* Equation (3.17) overestimates the fluorescence gain as it assumes the maximum possible value. The actual gain builds up over time through the collisional transfer of population to level 2. The importance of this was pointed out in Ref. 16.

Contributions to the Raman gain also come from two terms. Unlike the fluorescence, both terms in Eq. (3.11c) are positive. Raman light grows through stimulated emission from the upper state, proportional to the 2-3 inversion, and also through a two-photon contribution, proportional to

$$|\Omega_P|^2/4\beta_{31}\Delta_P^2 .$$

The relative importance of these terms can be found by taking their ratio. With the approximation (3.14) and the requirement (3.4) it is easy to show that the two-photon term is dominant while the pump pulse acts. Under this condition we can write the Raman gain as

$$g_R = \kappa_R \frac{|\Omega_P|^2}{2\beta_{31}\Delta_P^2} . \tag{3.18}$$

This is the usual expression for the steady-state Raman gain coefficient.[4] In other words, the collisional transfer of population has no influence on the growth of Raman light during the duration of the pump pulse.

However, once the pump pulse ends, only the inversion term is nonzero, and so it makes a small contribution. It may seem puzzling that Raman scattering, which is thought of as a two-photon process, can be generated through a one-photon transition. However, this is just amplification in the far wing of the collision-broadened 2-3 transition line.

The ratio of gain coefficients of the fluorescence and Raman pulses during pumping now can be found from Eqs. (3.17) and (3.18):

$$\frac{g_F}{g_R} = \frac{s_{22}-s_{33}}{\beta_{32}} 4\beta_{31} \frac{\Delta_P^2}{|\Omega_P|^2}, \quad 0 \le \tau \le \tau_P \tag{3.19}$$

or, employing the approximation (3.14),

$$\frac{g_F}{g_R} = \frac{2\beta_{31}\beta_{21}}{\beta_{32}} \frac{1}{(A_{21}+A_{23})^2} ((A_{21}+2A_{23})\{1-\exp[-(A_{21}+A_{23})\tau]\} - A_{23}(A_{21}+A_{23})\tau) . \tag{3.20}$$

We have assumed $\kappa_F \simeq \kappa_R$ for simplicity. During the buildup of fluorescence, $(A_{21}+A_{23})\tau \ll 1$, Eq. (3.20) reduces to

$$\frac{g_F}{g_R} \simeq \frac{2\gamma_{31}\gamma_{21}}{\gamma_{32}} \tau , \tag{3.21}$$

where we have replaced the total dephasing rates by the collisional rates since we are in the rate-equation limit.

Equation (3.21) shows that the relative growth of the fluorescence and Raman pulses depends only on the collisional rates and the pump pulse duration, not on the Rabi frequency or the detuning. (This is not strictly true since we have assumed a constant pump. In the general case, τ is replaced by $\int_0^\tau \Omega_P d\tau'/\Omega_P$.) Assuming the collisional-broadening rates to be comparable in magnitude, we therefore expect fluorescence growth to dominate Raman growth when there is a large collisional transfer of population and the pump pulse has a long duration ($\gamma_{21}\tau_P \gg 1$).

After the pump pulse ends ($\tau > \tau_P$), only the 2-3 inversion terms contribute to the ratio of gain coefficients:

$$\frac{g_F}{g_R} \simeq \frac{\Delta_P^2}{\beta_{32}^2} , \tag{3.22}$$

which, from (3.4), shows that fluorescence gain dominates Raman gain after the pump pulse ends, as expected.

B. Coherence effects

Investigation of the OBE and Maxwell equations in the rate-equation limit has enabled us to see how the different one- and two-photon processes contribute to amplification. However, any coherence effects are completely damped out in this limit because of the large collision rates. These coherence effects arise through the interaction of the pump and Stokes fields with the population in the atoms and can lead to significantly different behavior in propagation than that predicted by simple gain theory. In particular, saturation effects can be caused by coherently driven Rabi oscillations of the population. To investigate these effects we can no longer assume the 2-3 inversion to be independent of propagation distance and therefore we will no longer restrict the Stokes components to be much smaller than the pump field in magnitude. We will, however, assume that only one or the other of the Stokes components is dominant on the 2-3 transition at any propagation distance. Therefore we will examine coherence effects for the Raman and fluorescence pulses separately.

1. Fluorescence component

To investigate the interaction of the fluorescence with the 2-3 inversion we will continue to assume that the pump pulse is undepleted during propagation. Also, since we are interested in coherence effects, we will ignore the damping of the fluorescence dipole and 2-3 inversion. This gives us a set of reduced equations:

$$\frac{\partial}{\partial\tau}s_{22}=\tfrac{1}{2}\beta_{21}\frac{|\Omega_P|^2}{\Delta_P^2}+\frac{i}{2}(f_{23}\Omega_F-f_{32}\Omega_F^*)\ , \tag{3.23a}$$

$$\frac{\partial}{\partial\tau}s_{33}=\frac{i}{2}(f_{32}\Omega_F^*-f_{23}\Omega_F)\ , \tag{3.23b}$$

$$\frac{\partial}{\partial\tau}f_{32}=-\frac{i}{2}\left[(s_{22}-s_{33})-\frac{1}{4}\frac{|\Omega_P|^2}{\Delta_P^2}\right]\Omega_F\ . \tag{3.23c}$$

The collisional transfer of population from the ground state to level 2 is an incoherent process. Thus the shape of the pump pulse should not be too important as long as the pump is smooth. We will assume a square pump pulse. We will also take the fluorescence field to be real (it is on resonance and we have ignored damping). Then the dipole will be in quadrature with the field. The notation

$$w=s_{22}-s_{33}\ , \tag{3.24a}$$

$$v=2if_{32}\ , \tag{3.24b}$$

$$\Gamma=\tfrac{1}{2}\beta_{21}\frac{|\Omega_P|^2}{\Delta_P^2}\ , \tag{3.24c}$$

$$\mu=\frac{1}{4}\frac{|\Omega_P|^2}{\Delta_P^2}\ , \tag{3.24d}$$

allows us to write Eqs. (3.23) as

$$\frac{\partial}{\partial\tau}w=\Gamma-v\Omega_F\ , \tag{3.25a}$$

$$\frac{\partial}{\partial\tau}v=(w-\mu)\Omega_F\ . \tag{3.25b}$$

This pair of equations is equivalent to those of a two-level atom incoherently pumped at the rate Γ and interacting with a radiation field Ω_F, with damping of the dipole proportional to the field.

The general solution of Eqs. (3.25), with the initial conditions $w(z,0)=v(z,0)=0$, is

$$w(z,\tau)=\mu\{1-\cos[\Theta(z,\tau)]\}+\Gamma\int_0^\tau\cos[\Theta(z,\tau)-\Theta(z,\tau')]d\tau'\ , \tag{3.26a}$$

$$v(z,\tau)=-\mu\sin[\Theta(z,\tau)]+\Gamma\int_0^\tau\sin[\Theta(z,\tau)-\Theta(z,\tau')]d\tau'\ , \tag{3.26b}$$

where

$$\Theta(z,\tau)=\int_0^\tau\Omega_F(z,\tau')d\tau'\ . \tag{3.26c}$$

The situation described by Eqs. (3.26) is shown in Fig. 3. The pump transfers population to level 2 for a time τ_0 before the fluorescence appears and continues to do so as the fluorescence interacts with the atom. We can explicitly include these conditions in Eqs. (3.26):

$$w(z,\tau)=\begin{cases}\Gamma\tau, & 0\le\tau\le\tau_0\\ (\Gamma\tau_0-\mu)\cos[\Theta(z,\tau)]+\mu+\Gamma\int_{\tau_0}^\tau\cos[\Theta(z,\tau)-\Theta(z,\tau')]d\tau', & \tau_0\le\tau\le\tau_P\end{cases} \tag{3.27a}$$

$$v(z,\tau)=\begin{cases}0, & 0\le\tau\le\tau_0\\ (\Gamma\tau_0-\mu)\sin[\Theta(z,\tau)]+\Gamma\int_{\tau_0}^\tau\sin[\Theta(z,\tau)-\Theta(z,\tau')]d\tau', & \tau_0\le\tau\le\tau_P\ .\end{cases} \tag{3.27b}$$

The integrals can be evaluated explicitly only for very few special cases, the simplest of which is when $\Omega_F(z,\tau>\tau_0)$ has a constant value, Ω_F^0:

$$w(z,\tau)=\begin{cases}\Gamma\tau, & 0\le\tau\le\tau_0\\ (\Gamma\tau_0-\mu)\cos[A(z,\tau)]+\mu+\dfrac{\Gamma(\tau-\tau_0)}{A(z,\tau)}\sin[A(z,\tau)], & \tau_0\le\tau\le\tau_P\end{cases} \tag{3.28a}$$

$$v(z,\tau)=\begin{cases}0, & 0\le\tau\le\tau_0\\ (\Gamma\tau_0-\mu)\sin[A(z,\tau)]+\dfrac{\Gamma(\tau-\tau_0)}{A(z,\tau)}\{1-\cos[A(z,\tau)]\}, & \tau_0\le\tau\le\tau_P\end{cases} \tag{3.28b}$$

where $A(z,\tau)$ is the "area" of the fluorescence pulse,

$$A(z,\tau)=\Omega_F^0(\tau-\tau_0)\ . \tag{3.28c}$$

Comparing the behavior of the atom in the time regime $\tau_0\le\tau\le\tau_P$ to that of the usual two-level atom reveals some interesting features.

The first term in each equation (3.28a) and (3.28b) is the solution of the standard two-level-atom model,[19] with the replacement $\Gamma\tau_0\to1$, $\mu\to0$. The last term shows how the usual dynamics are modified due to the incoherent

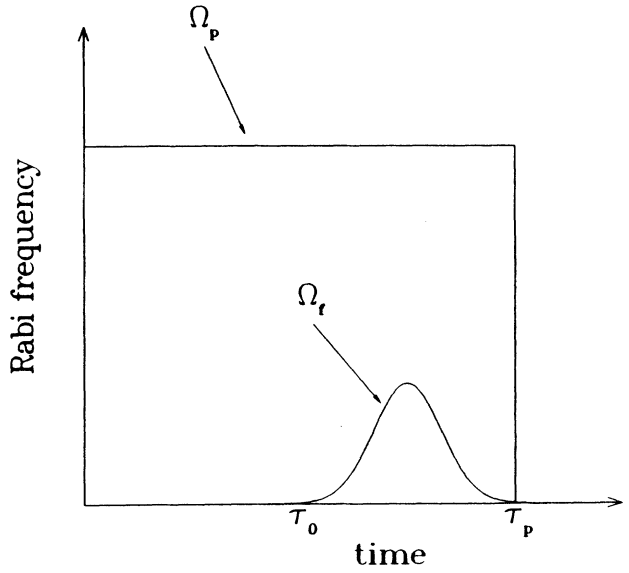

FIG. 3. Situation described by Eqs. (3.26). Pump pulse Ω_P acts for a time τ_0 populating upper state before fluorescence Ω_F begins.

pumping.

Because the inversion is initially positive, the fluorescence will grow. From the McCall-Hahn area theorem[25] for two-level atoms, we expect a weak probe to grow to a stable area of π. This is because all the population in the upper state will be transferred to the lower state by a π pulse with no remaining coherence in the atom to drive the field. For the pumped atom, we find from Eqs. (3.28) that for a π fluorescence pulse

$$w(A=\pi)=-\Gamma\tau_0+2\mu\ , \tag{3.29a}$$

$$v(A=\pi)=\frac{2}{\pi}\Gamma(\tau-\tau_0)\ . \tag{3.29b}$$

This says that most of the initial available population ($\Gamma\tau_0$) is now in the lower state, while some (2μ) remains in the upper state because of the absorptive part of the dipole. Some energy which has been pumped into the atom during the π-pulse interaction has ended up in the dipole. Therefore, a π pulse is no longer stable in this situation. This can also be seen from the fact that the second term in (3.28b) is proportional to

$$\cos^2[A(z,\tau)/2]\ ,$$

which has period 2π, not π.

For a 2π fluorescence pulse we find

$$w(A=2\pi)=\Gamma\tau_0\ , \tag{3.30a}$$

$$v(A=2\pi)=0\ . \tag{3.30b}$$

Therefore the population returns to the upper state and there is no residual coherence, so the 2π pulse will be stable. However, comparison of Eqs. (3.30) to the initial conditions of the atom before the fluorescence starts, Eqs. (3.28), reveals the surprising fact that even though the atom is continually pumped while it is interacting with the fluorescence, it ends up precisely in its initial state after passage of the 2π fluorescence pulse. In other words, *all of the energy transferred to the atom must end up in the field through propagation effects.* Since we expect the 2π pulse to be stable, this implies a strong reshaping of the fluorescence as it evolves. As more energy gets into the field, the pulse will sharpen, growing narrower and higher.

This result cannot be true in general, however. Equation (3.30a) says the result is independent of Γ, which becomes larger as collisional broadening is increased. This clearly cannot be, as strong collisions will cause damping of the dipole (an effect we have ignored in this simple model). In addition, the reinverted atom is in an unstable state and will begin to decay. We will see in the numerical studies that although a 2π pulse is not stable, it is "quasistable" in the sense that although it attempts to retain its area of 2π, additional peaks develop after its passage which cause the combined fluorescence area to grow to multiples of 2π.

In this approximate analysis of coherence effects in the fluorescence, we have used a very simple model. The assumption of a square fluorescence pulse cannot be justified in discussing the propagation properties of the fluorescence. As we will see in Sec. IV, the propagation of fluorescence is a great deal more complicated in the general case. It may be perhaps surprising, therefore, that such a simple model will be able to describe some of the basic features of coherence effects in the fluorescence.

2. *Raman component*

For the investigation of coherence effects in the Raman light, we can no longer assume nondepletion of the pump pulse since the Raman scattering results from a two-photon process. However, we will now assume that we can ignore population transfer to level 2 and spontaneous decays, i.e., $|\beta_{jk}/\Delta_P|\rightarrow 0$ and $A_{jk}\tau\ll 1$. Then the relevant equations becomes

$$\frac{\partial}{\partial\tau}s_{11}=\frac{i}{2}(\Omega_{TP}^{*}r_{13}-\Omega_{TP}r_{31})\ , \tag{3.31a}$$

$$\frac{\partial}{\partial\tau}s_{33}=\frac{i}{2}(\Omega_{TP}r_{31}-\Omega_{TP}^{*}r_{13})\ , \tag{3.31b}$$

$$\frac{\partial}{\partial\tau}r_{31}=-(\beta_{31}+i\Delta')r_{31}-\frac{i}{2}\Omega_{TP}^{*}(s_{11}-s_{33})\ , \tag{3.31c}$$

where

$$\Omega_{TP}=\frac{\Omega_P\Omega_R^{*}}{2\Delta_P} \tag{3.31d}$$

is called the two-photon Rabi frequency and

$$\Delta'=\frac{|\Omega_R|^2-|\Omega_P|^2}{4\Delta_P} \tag{3.31e}$$

is the ac Stark shift. Equations (3.31) form the basis of the two-photon vector model[26] and have been extensively used to describe off-resonant interactions in three-level systems.[27–29]

Two basic types of coherence effects can be obtained from these equations. The first, and better known, are

two-photon Rabi oscillations.[28] We can obtain this result if we assume that damping and the ac Stark shift are negligible. Then Eqs. (3.31a)–(3.31c) are formally identical to the equations for a two-level atom driven on resonance and admit the solution

$$w_{13}=\cos[A_{\mathrm{TP}}(z,\tau)]\ , \tag{3.32a}$$

$$v_{13}=\sin[A_{\mathrm{TP}}(z,\tau)]\ , \tag{3.32b}$$

where

$$A_{\mathrm{TP}}(z,\tau)=\int_0^{\tau}\Omega_{\mathrm{TP}}(z,\tau')d\tau' \tag{3.32c}$$

is the two-photon area and

$$w_{13}=s_{11}-s_{33}\ , \tag{3.32d}$$

$$v_{13}=2\,\mathrm{Im}(r_{13})\ . \tag{3.32e}$$

We have implicitly taken the pump and Raman fields to be real. Therefore the population inversion and coherence oscillate sinusoidally and thus the two-photon Rabi frequency will experience coherence effects, just as the fluorescence does on the 2-3 transition. However, the manifestation of these oscillations is different from the fluorescence case since both the pump and Raman fields must vary.

The second coherence effect is due to the propagation of the two-photon Rabi frequency. The following Maxwell equation describes propagating of the two-photon field:

$$\frac{\partial}{\partial z}\Omega_{\mathrm{TP}}=\frac{i}{\Delta_P}\left\{\Omega_{\mathrm{TP}}[\kappa_P(s_{11}-s_{22})+\kappa_R(s_{22}-s_{33})]+\frac{1}{\Delta_P}(\kappa_P|\Omega_R|^2-\kappa_R|\Omega_P|^2)r_{13}\right\}\ . \tag{3.33}$$

This can be separated into two equations for the field amplitude and phase:

$$\frac{\partial}{\partial z}R=\frac{1}{2\Delta_P^2}(\kappa_P|\Omega_R|^2-\kappa_R|\Omega_P|^2)(u_{13}\sin\phi-v_{13}\cos\phi)\ , \tag{3.34a}$$

$$R\frac{\partial}{\partial z}\phi=\frac{1}{2\Delta_P}R[\kappa_P(s_{11}-s_{22})+\kappa_R(s_{22}-s_{33})]+\frac{1}{2\Delta_P^2}(\kappa_P|\Omega_R|^2-\kappa_R|\Omega_P|^2)(u_{13}\cos\phi+v_{13}\sin\phi)\ , \tag{3.34b}$$

where

$$\Omega_{\mathrm{TP}}=Re^{i\phi},\quad r_{13}=\tfrac{1}{2}(u_{13}+iv_{13})\ . \tag{3.34c}$$

We now look at the phase of the field. If we disturb the phase by a small amount, $\phi\rightarrow\phi+\delta\phi$, we can relate the change in phase increment to the change in amplitude:

$$\frac{\partial}{\partial z}\delta\phi=-\left[\frac{1}{R}\frac{\partial R}{\partial z}\right]\delta\phi\ . \tag{3.35}$$

Thus a small change in phase will become unstable when the two-photon Rabi frequency is decreasing, i.e., $\partial R/\partial z$ is negative. This effect will be most important at points where R is small. We can therefore expect phase instabilities near the tail end of the pump pulse when either the pump or the Raman pulse is being absorbed. This phase instability will cause a change in sign of the part of the two-photon Rabi frequency which is being absorbed.[30,31] This consequently implies a decrease in the two-photon area with a corresponding modification of how population is transferred between levels 1 and 3.

We will find in the numerical studies that one or the other of these two coherence effects (strong two-photon Rabi oscillations or phase instabilities) will be dominant during propagation. Which effect will be more important can be understood from a discussion of saturation effects in transient SRS given by Elgin and O'Hare.[32] They define a nonlinear time function T which can be written in our notation as (approximately)

$$T(\tau)\equiv\left|\frac{\mathbf{d}_{23}\cdot\mathbf{e}_S}{\mathbf{d}_{21}\cdot\mathbf{e}_P}\right|\frac{1}{2\Delta_P}\int_0^{\tau}|\Omega_P(z=0,\tau')|^2d\tau'\ . \tag{3.36}$$

$T(\tau)$ is closely related to the two-photon area, A_{TP}. Indeed, for the special case where

$$E_R(z=0,\tau)=E_P(z=0,\tau)\ ,$$

they are identical.

Interpreting the limits $T(\tau\rightarrow\infty)\ll 1$ and $T(\tau\rightarrow\infty)\gg 1$ as "low input pump energy" and "high input pump energy," respectively, Elgin and O'Hare discuss the different behavior of the system based on the amount of energy in the input pump pulse. For low input pump energy they show that the pump pulse envelope oscillates around $\Omega_P=0$ as it develops and eventually all the pump energy is converted into Raman energy. This corresponds to the development of phase shifts in the pump pulse through the instabilities we have discussed. In the limit of large input pump energy, they show that population oscillations are important, corresponding to the two-photon Rabi oscillations.

These results lead to a fairly simple physical interpretation. If the input pump energy is large enough, the two-photon area will develop to be greater than π before absorption of the tail end of the pump pulse can lead to phase instabilities. Then population transferred to level 3 will begin to be returned to level 1, implying an amplification of the pump light toward the tail end of the pump pulse, giving stable growth. If the input pump energy is too small, this will not happen and phase shifts will be dominant.

IV. NUMERICAL SIMULATIONS

We are interested in features of Stokes amplification that are due to nonlinear effects. Some of the terms

which contribute to these effects (such as Stokes competition through the 2-3 inversion) were left out of our analytic limits. To investigate the nonlinear behavior of the system, we will return to Eqs. (2.8) and (2.11) and integrate them numerically.

To obtain realistic parameters for our numerical investigations, we will base our three-level system on atomic thallium. This is the system used by Raymer and Carlsten in their investigation of SRS and stimulated collision-induced fluorescence.[13–16] We have successfully used our model to obtain qualitative and quantitative agreement with the results of some of these experiments.[33] A discussion of the atom is given in Appendix B.

We will take our pump pulse to have a Gaussian temporal shape. We will take the pump pulse width [amplitude full width at half maximum (FWHM)] to be $\tau_P = 10$ ns. We will assume very weak Gaussian Stokes probes of intensity 10 nW/cm^2 and temporal width of $10\tau_P$. These will be initially centered under the pump pulse. All other relevant physical parameters will be given in the figure captions.

In many cases, the growths of the fluorescence and Raman components proceed independently until the pulses become comparable in magnitude. We begin by examining each pulse separately.

A. Fluorescence component

A typical result of the amplification of fluorescence before the Raman pulse becomes large is shown in Fig. 4. The collisional broadening has been chosen moderately large ($\gamma_{21}\tau_P = 10$, $\gamma_{32}\tau_P = 1.0$, $\gamma_{31}\tau_P = 0.25$) so that fluorescence begins with a larger gain than that of the Raman component. Initially, the fluorescence peak is delayed toward the end of the pump pulse, a reflection of the time-dependent collisional transfer of population to the upper state. For $z < 0.08$ cm the spatial growth of the fluorescence is exponential as can be clearly seen in Fig. 5.

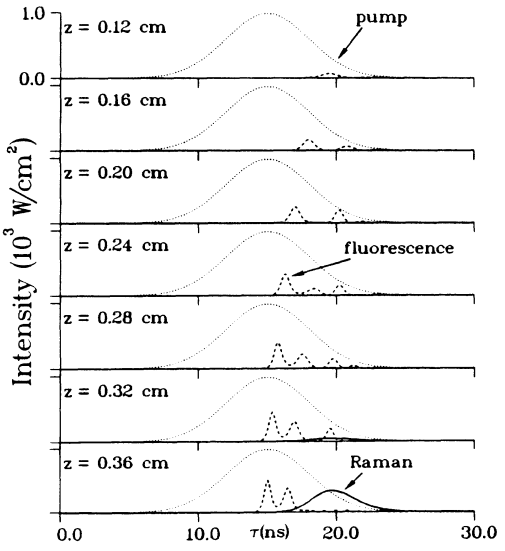

FIG. 4. Example of growth of fluorescence component showing ringing oscillations, development of 2π pulses, and saturation. Parameters are peak pump intensity, $I_0 = 2$ MW/cm^2, $\gamma_{21}\tau_P = 10$, $\gamma_{32}\tau_P = 1.0$, $\gamma_{31}\tau_P = 0.25$, $\Delta_P\tau_P = 2.0 \times 10^4$. Pump pulse is shown reduced by a factor 5×10^{-4}. Pulses are labeled by dotted line (pump), dashed line (fluorescence), and solid line (Raman).

By the distance 0.08 cm the fluorescence has grown large enough to start to induce coherent response in the 2-3 transition. This marks the beginning of the saturation of the fluorescence. The first effects of nonlinear behavior are seen for $0.12 \leq z \leq 0.16$ cm as the fluorescence drives population from level 2 to level 3. This results in the development of additional peaks at the tail end of the fluorescence. This is analogous to the well-known Burnham-Chiao[6,34] ringing seen in a two-level amplifier. The amplitude of each generated peak has the opposite sign of the one before it, the first being positive. The ringing develops as energy is exchanged back and forth between the atoms and the fluorescence.

Propagation of the ringing oscillations is seen up to 0.16 cm. The leading edge of the fluorescence is amplified and advances underneath the pump. By 0.16 cm the first fluorescence peak has grown to an area of 2π. The 2π pulse is expected to be quasistable, as discussed in Sec. III. This is evident in the propagation from 0.16 to 0.20 cm where the first peak starts to pull away (toward small times) from the second. The first peak leaves no coherence after its passage to aid the advancement of the second peak.

Eventually, however, some fluorescence starts to develop between the two peaks ($z = 0.24$ cm) due to the repumping of level 2. Since the first peak returns the atom to its initial state, the new peak develops like the first. That is, the new peak grows to an area of 2π and starts to pull away from the following peak.

It should be noted that this newly generated "ringing" is different in character from the normal Burnham-Chiao ringing. Each subpulse (at $\tau = 16$ ns and $\tau = 17.5$ ns at

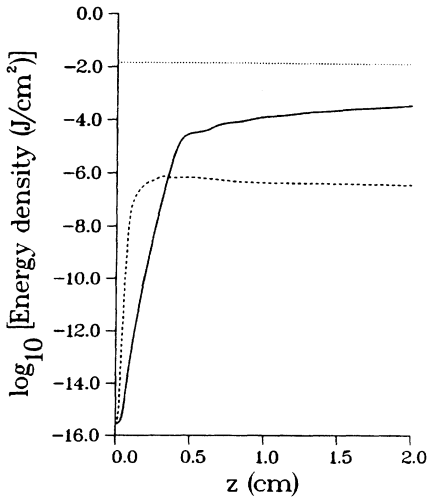

FIG. 5. Growth of energy in Stokes components for simulations of Figs. 4 and 8. Pulses labeled as in Fig. 4.

$z=0.28$ cm) has a fairly well-defined area of 2π. Also, the amplitude of the new peak at $\tau=17.5$ ns has the same sign as the previous peak at $\tau=16$ ns (the valley between the peaks does not go down to zero) and it is generated *while the atom is being pumped.* This is not the case for the initial ringing which develops after the pump pulse ends.

This behavior of the development of a series of 2π peaks continues as the propagation proceeds until the Raman pulse starts to amplify strongly at approximately 0.32 cm. It induces a direct transfer of population from the ground to the excited state, causing the 2-3 inversion to become negative. The fluorescence dipole then becomes absorptive and consequently the fluorescence that falls underneath the Raman pulse begins to decrease (0.36 cm).

The various stages of propagation just described are general features of the fluorescence growth. The degree to which each occurs depends strongly upon the physical parameters of the simulation. An example of this, showing the dependence of the fluorescence component on the parameters which are important for the collisional transfer of population, is shown in Fig. 6. Here, the pump intensity has been reduced by a factor of 10 and the collisional-broadening rates have been increased by a factor of 10 from those in Fig. 4. This is an example of the rate-equation limit for the fluorescence. The fluorescence growth is very similar to that of Fig. 4 except that the distinction between peaks is somewhat washed out due to the rapid dipole dephasing. The most important aspect of this example, however, is seen in Fig. 7. Comparison of this figure to Fig. 5 shows that, before saturation, the energy growth in the fluorescence pulse is almost identical in both cases. This is because, although we have independently varied the pump intensity and collisional rates, we have chosen their product to remain constant. The amount of population transferred to level 2 and, thus, available for amplification of the fluorescence, is directly proportional to $\beta_{21}|\Omega_P|^2/\Delta_P^2$ [see Eq. (3.14)]. The constancy of this factor yields the same overall transfer of energy to the fluorescence in both simulations. It should also be noted that, although the fluorescence growth has remained the same, the Raman growth is significantly different because of the decrease in pump intensity and increase of the collision rates.

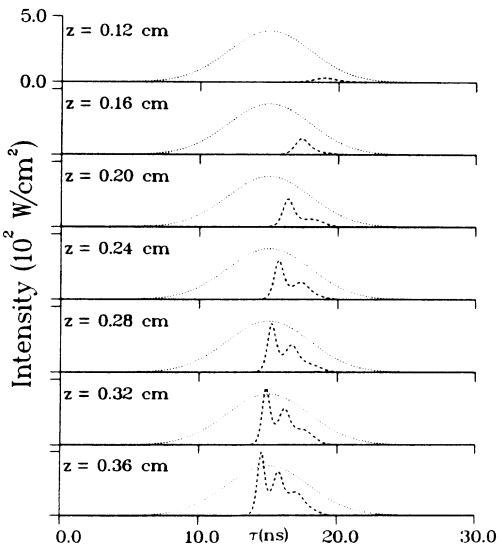

FIG. 6. Growth of fluorescence component in an amplifier with ten times the broadening of that in Fig. 4 and $I_0=0.2$ MW/cm^2. Pump shown reduced by a factor 2×10^{-3}. Pulses labeled as in Fig. 4.

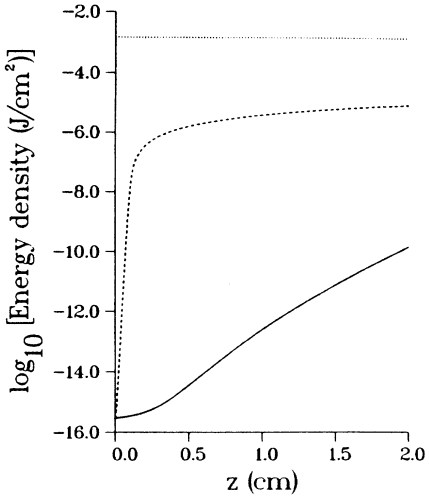

FIG. 7. Growth of energy in Stokes components for simulation of Fig. 6. Pulses labeled as in Fig. 4.

The different stages of fluorescence development can be summarized as follows. Initial exponential growth occurs most strongly in the trailing edge of the pump pulse since the upper level is populated gradually, by collisions. The 2-3 transition acts like a two-level amplifier causing the development of ringing oscillations. The leading edge of the fluorescence eventually advances underneath the pump pulse and a sequence of 2π-type pulses is generated. These coherence effects play a fundamental role in determining the amount of pump energy which can be converted to the fluorescence. The Rabi oscillations can cause a self-saturation of the fluorescence or, alternatively, the fluorescence growth can be cut off by the rapidly rising Raman component.

B. Raman component

From our discussion in Sec. III B 2, we expect to see different behavior in the Raman component, depending upon the amount of initial pump energy. Our first example (Fig. 8) is a continuation of the propagation begun in Fig. 4. The initial growth of the Raman light is delayed toward the end of the pump pulse due to the transient Raman effect.[3] As the Raman pulse amplifies, it advances under the pump and additional peaks develop in its tail. A similar behavior was observed for the fluorescence. Here, the development of peaks is due to two-photon Rabi oscillations of population between levels 1 and 3. The signature of these oscillations can be seen in the small dips of intensity of the pump pulse which corre-

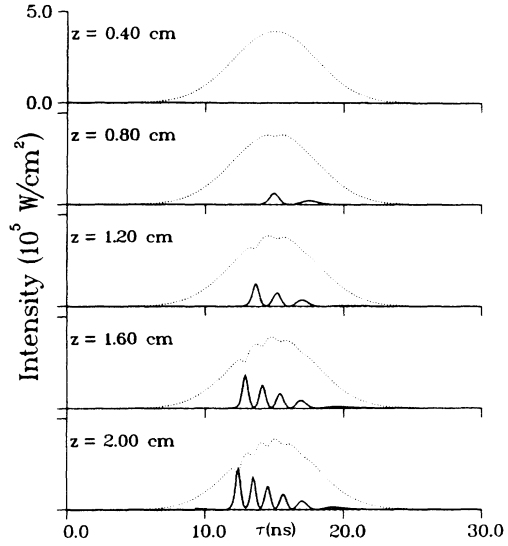

FIG. 8. Continuation of simulation of Fig. 4 showing development of Raman component. Self-modulation of the pump and Raman light is caused by coherent two-photon Rabi oscillations. Pump shown reduced by a factor 0.2. Pulses labeled as in Fig. 4.

spond to peaks in the Raman pulse. As in the case of fluorescence, these oscillations lead to a saturation of the amplifying component (see Fig. 5).

Based solely upon our discussion of gain coefficients in Sec. III A, we might expect that if we adjust the pump intensity and detuning so as to keep $|\Omega_P|/\Delta_P$ constant, the growth of the Raman light will not change. That this is not so is illustrated in Fig. 9. Here we have decreased the pump amplitude and detuning each by a factor of 10. Although the Raman gain coefficient remains the same, the absorption of the pump is quite different. In the simulation of Fig. 8, $T(\tau\rightarrow\infty)\simeq 1.8$, corresponding to two-photon Rabi oscillations. Here, $T(\tau\rightarrow\infty)\simeq 0.18$, and the pump development is marked by phase instabilities. If we were to continue the propagation past $z=2.0$ cm, eventually all of the remaining pump light would be converted to Raman light.

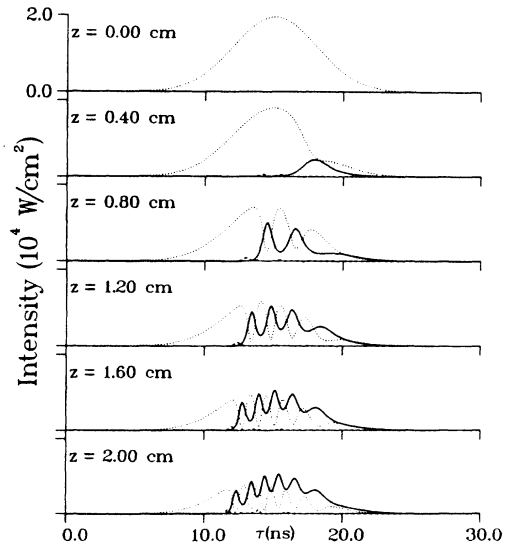

FIG. 9. Development of Raman component in a system where the pump amplitude and detuning have been decreased by a factor of 10 from Fig. 8. Self-modulation of the pump and Raman light is caused by phase instabilities in the pump. Pulses labeled as in Fig. 4.

An interesting consequence of this type of behavior is that, as more of the pump light is converted into Raman light, less and less of the population is transferred from level 1 and to level 3. The reason for this can be understood from the behavior of the two-photon area, $A_{\rm TP}$. As the pump propagates, it develops several phase changes over its temporal duration. These become more numerous with propagation distance. Each phase reversal changes the sign of the two-photon Rabi frequency which occurs in the definition of $A_{\rm TP}$ [Eq. (3.32c)]. Consequently, the two-photon area alternately grows and decays. Since the phase changes occur more frequently at larger propagation distances, $A_{\rm TP}$ never is able to grow substantially before it starts to decrease (and vice versa). The result of this is that the two-photon area never strays far from zero, and the inversion, given by Eq. (3.32a), always remains close to 1.

This has an important effect on the Raman light. As more and more pump light is converted to Raman light, less and less population is transferred to level 3. Thus, after a significant fraction of the pump has been converted in this manner, the Raman light will propagate through a medium which is almost transparent to it, even though there are very strong coherent interactions occurring.

C. Interaction of the Stokes components

So far we have described the coherent development of the fluorescence and Raman components separately. We have seen some evidence of the interaction of the pulses and we discuss this now in more detail.

The most important interaction between the components occurs when the Raman component grows to values comparable to the fluorescence. This causes a suppression of the fluorescence by creating a negative inversion in the 2-3 transition and, consequently, an absorptive dipole (see, e.g., $z=0.36$ cm in Fig. 4 and $z>0.4$ cm in Fig. 5). This mechanism also traps population in the upper state. The suppression of the fluorescence component by the Raman component will be most important at lower pressures since then the fluorescence grows more slowly and the Raman light more rapidly. It is possible, of course, for the Raman component to dominate completely the fluorescence component at low pressures so that the latter never amplifiers. This type of behavior has been observed.[16]

An additional interaction between the components has also appeared in the numerical simulations but has not been commented on. It results from the behavior of the populations at large propagation distances in the limit of low input pump energy. When the Raman pulse

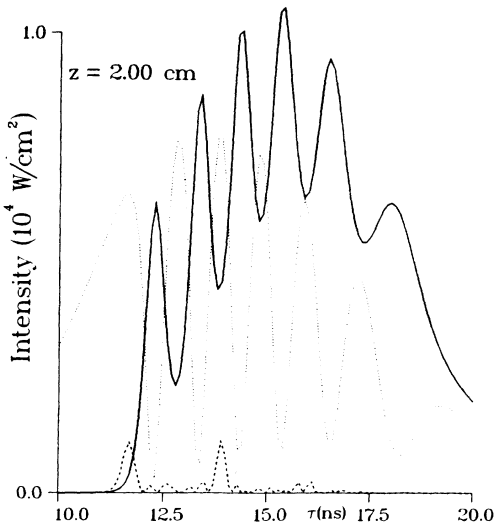

FIG. 10. Enlargement of $z=2.0$ cm in Fig. 9 showing additional amplification of the fluorescence component under valleys in the Raman component. Pulses labeled as in Fig. 4.

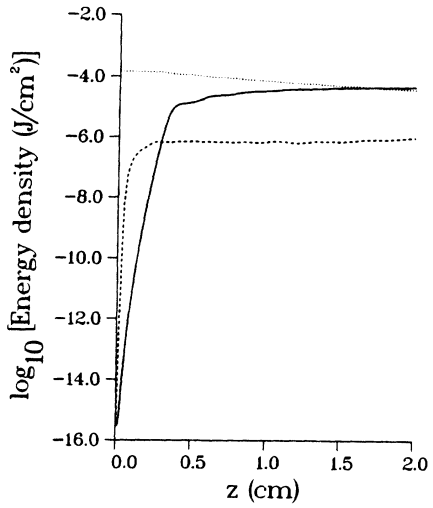

FIG. 11. Growth of energy in Stokes components for simulation of Fig. 9. Pulses labeled as in Fig. 4.

amplifies, the population which was transferred by collisions to level 2 becomes trapped in the upper state. However, as discussed in Sec. IV B above, when the development of the pump pulse is marked by phase shifts, less and less population is transferred to level 3 at large propagation distances. It is therefore possible that eventually the 2-3 inversion will again become positive at times, leading to additional fluorescence growth. Figure 10 shows an enlargement of $z=2.0$ cm in Fig. 9, where this effect is clearly visible: valleys in the Raman intensity are accompanied by peaks in the fluorescence intensity. This behavior can lead to a gradual rise in the fluorescence after its suppression by the Raman light (Fig. 11).

Although it is usually the Raman component which affects the fluorescence component, it is possible at high pressures for the reverse to happen, although somewhat indirectly. If the fluorescence component grows quickly enough, much of the pump light can be converted to fluorescence before the Raman component becomes stimulated. In effect, the continual depletion of the pump causes the Raman gain to decrease with distance. Although this effect is possible, we have found it to be rare in our simulations. The reason is that the fluorescence must grow to a noticeable fraction of the pump before it saturates. However, saturation of the fluorescence occurs very early in the propagation, usually well before depletion of the pump is noticeable.

V. INHOMOGENEOUS BROADENING EFFECTS

Until now we have ignored the inhomogeneous broadening which results from the range of velocities of the atoms of the gas and is described by the Doppler line shapes [Eq. (A9) in Appendix A]. Although the inhomogeneous broadening does not change the fundamental physical processes which occur in the atom-field interactions, it introduces additional damping in the system which leads to a delay in the pulse developments.

To discuss the effects of inhomogeneous broadening, we must calculate the averaged coherences $\langle s_{12}\rangle_{\Delta_{21}}$, $\langle f_{32}\rangle_{\Delta_{23}}$, and $\langle r_{32}\rangle_{\Delta_{23}}$. We will do this only in the rate-equation limit. Also, we will confine ourselves to calculations of the imaginary parts of the dipoles, since these are responsible for the gain.

To ensure that the Stokes components are well separated spectrally, we must assume, in addition to (3.4), that

$$|\Delta_P^0 T_{jk}^*| \gg 1 \ . \tag{5.1}$$

Then, using the Doppler line shapes (A9), a simple calculation shows

$$\mathrm{Im}\langle s_{12}\rangle_{\Delta_{21}} = -\frac{1}{2} T_{21}^* H(\beta_{21} T_{21}^*/\sqrt{\pi},\ -T_{21}^* \Delta_P^0/\sqrt{\pi}) \ , \tag{5.2a}$$

$$\mathrm{Im}\langle f_{32}\rangle_{\Delta_{23}} = -\frac{1}{2} T_{23}^* H(\beta_{32} T_{23}^*/\sqrt{\pi},\ -T_{23}^* \Delta_S^0/\sqrt{\pi}) \left[(s_{22}-s_{33}) - \frac{1}{4}\frac{|\Omega_P|^2}{(\Delta_P^0)^2}\right]\Omega_F \ , \tag{5.2b}$$

$$\mathrm{Im}\langle r_{32}\rangle_{\Delta_{23}} = -\frac{1}{8} H\left[\frac{T_{21}^* T_{23}^* \beta_{31}/\sqrt{\pi}}{T_{21}^* - T_{23}^*},\ -\frac{T_{21}^* T_{23}^* \Delta_S^0/\sqrt{\pi}}{T_{21}^* - T_{23}^*}\right]\frac{T_{21}^* T_{23}^*}{|T_{21}^* - T_{23}^*|}\frac{|\Omega_P|^2}{(\Delta_P^0)^2}\Omega_R \ , \tag{5.2c}$$

where $H(a,v)$ is the Voigt function which describes the contributions of both homogeneous and inhomogeneous broadening to the absorption line profile:[35]

$$H(a,v)=\frac{a}{\pi}\int_{-\infty}^{\infty}\frac{e^{-x^2}}{(v-x)^2+a^2}dx \ . \tag{5.3}$$

A considerable simplification occurs for the pump dipole when we employ (5.1). We find

$$\mathrm{Im}\langle s_{12}\rangle_{\Delta_{21}}=-\frac{1}{2}\frac{\beta_{21}}{(\Delta_P^0)^2}\Omega_P \ . \tag{5.4}$$

This same expression results when we ignore the Doppler broadening. This gives the important result that, when the Stokes components are well separated in the output spectrum, the collisional transfer of population to the upper level is insensitive to inhomogeneous broadening effects. In other words, *inhomogeneous broadening does not affect the amount of energy which is made available for the fluorescence growth.*

Both the fluorescence and Raman components are affected by the inhomogeneous broadening. The dominant type of damping which occurs in their growth is influenced by the ratio of the inhomogeneous and Doppler linewidths. When $\beta_{32}T_{23}^{*}\gg 1$, the fluorescence growth is dominated by collisional broadening. In this case, Eq. (5.2b) reduces to our previous result, Eq. (3.8a). When Doppler broadening dominates collisional broadening, the gain coefficient for fluorescence growth is given by Eq. (3.11b), with the replacement $\beta_{32}\rightarrow 1/T_{23}^{*}$.

The effect of inhomogeneous broadening is somewhat different for the Raman component. This is because Doppler effects from both the 1-2 and 2-3 transitions are important since the Raman scattering results from a two-photon process. The combinations of inhomogeneous lifetimes occur in Eq. (5.2c) because the detunings of the different transitions are related through a common velocity:

$$\frac{\Delta_P-\Delta_P^0}{\Delta_S-\Delta_S^0}=\frac{T_{23}^{*}}{T_{21}^{*}}=\frac{\omega_{21}^0}{\omega_{23}^0} \ . \tag{5.5}$$

Since the ratio of Doppler lifetimes is the inverse ratio of the natural frequencies of the transitions, we see that for small frequency shifts, inhomogeneous broadening is not an important effect for Raman scattering copropagating with the pump beam. This partial cancellation of the Doppler effect is analogous to the mechanism that occurs in Doppler-free spectroscopy.

Numerical simulations verify the behavior of the different field components discussed above. In particular, when the pump and fluorescence transitions are dominated by Doppler broadening, the fluorescence still saturates with approximately the same amount of energy as in the Doppler-free case, although the spatial fluorescence growth is slower. In addition, a change in the relative development of the Stokes components can occur when there is a small frequency shift in the Raman transition. This happens because the Raman component will be relatively insensitive to the Doppler broadening, while the fluorescence component will be strongly damped. Consequently, the Raman component can suppress the fluorescence component earlier in the propagation, as compared to the Doppler-free case. This can result in more energy being delivered to the Raman pulse.

VI. DISCUSSION

It is apparent from our analytic and numeric work that the individual development of the Stokes components and their interaction depend in a complicated but understandable way on the physical parameters of the problem. We have seen an example where an appropriate change of parameters has led to a negligible change of one component and a strong suppression of the other (Fig. 7) or where different parameters which give the same steady-state gain coefficient result in a complete change of behavior in the saturated regime (Fig. 9). Although the full description of the propagation depends on several independent parameters, general features of the pulse developments can be understood from the relationships between different times scales and the pulse amplitudes.

The initial (exponential) growth of both pulses depends on the amount of population available for the two processes. Population transferred by collisions to level 2 serves as the source for the fluorescence, while a "coherent population" of the virtual level set up by the pump is the source for the Raman scattering. Because the fluorescence amplification results from a one-photon transition, it will in general amplify more quickly than the two-photon Raman process when there is a significant collision-induced population transfer to level 2. The population transfer is also time dependent so that both long pump pulses and rapid collisions will favor fluorescence growth.

Under these conditions, the amplifying fluorescence will quickly saturate due to coherent interactions (Rabi oscillations) which develop in the 2-3 transition when the fluorescence has grown to an area of approximately π. The saturation limits the rate at which the fluorescence can amplify. Since the population transferred by collisions is generally much smaller than the ground-state population, the fluorescence usually has little effect on the amplification of the Raman light. The opposite is not true, however, for when the Raman pulse is amplified, it transfers population directly to level 3, creating a negative 2-3 inversion and, consequently, an absorptive fluorescence dipole.

The coherent development of the fluorescence shows some interesting features after saturation. As the propagation proceeds, the fluorescence advances underneath the pump pulse, the leading edge of the fluorescence encountering undepleted population of the upper level until the fluorescence reaches the beginning of the pump pulse. This can be likened to the interaction of a field with a two-level atom whose upper-state population is continually replenished. This results in the development in the fluorescence of a train of quasistable 2π pulses whose passage leaves the atom undisturbed.

The Raman component, too, can exhibit coherent effects after sufficient amplification. In a manner analogous to the saturation of the fluorescence, the Raman

light can induce two-photon coherent Rabi oscillations in the 1-3 transition. Although the Raman light cannot exhibit the development of a train of 2π pulses, another coherent effect can manifest itself due to the fact that the virtual population is affected by the development of the pump pulse. For a low-energy input pump pulse, phase instabilities in the pump can develop during propagation which drastically change the coherent atomic dynamics. This effect results in a complete transfer of energy from the pump to the Raman pulse while the population ultimately remains in level 1.

The two Stokes components interact with each other through the 2-3 inversion. By far the most important effect is the suppression of the fluorescence component by the Raman component after the latter transfers population directly from level 1 to level 3. However, the fluorescence component can still amplify gradually when phase instabilities occur in the pump pulse, due to the propensity of the population to return to the ground state at longer propagation distances.

ACKNOWLEDGMENTS

We thank J. L. Carlsten, J. Cooper, M. A. Johnson, B. Greenwood, M. J. Konopnicki, L. Matulic, and B. W. Shore for many helpful discussions during the course of this work. Financial support was provided by the U.S. Department of Energy and computational resources were made available by the John von Neumann Computing Center.

APPENDIX A: DERIVATION OF THE EQUATIONS OF MOTION

Our working set of atomic equations (2.8) has been derived from the usual three-level optical Bloch equations. The reduced Maxwell equations (2.11) were obtained from the one-dimensional propagation equation. Here we supply the details of the derivations of these equations which were omitted in Sec. II.

The equations of motion for the atomic operators are obtained from the Heisenberg equations of motion

$$i\hbar\frac{\partial}{\partial t}\hat{\sigma}_{jk}=[\hat{\sigma}_{jk},\hat{H}]\ , \tag{A1}$$

where the atomic Hamiltonian, in the dipole approximation, is given by

$$\hat{H}=\hat{H}_A+\hat{H}_I = \sum_{n=1}^{3}\hbar\omega_n\hat{\sigma}_{nn}-\hat{\mathbf{d}}\cdot\mathbf{E}\ . \tag{A2}$$

The OBE are derived through the use of the commutation relations

$$[\hat{\sigma}_{jk},\hat{\sigma}_{lm}]=\hat{\sigma}_{jm}\delta_{kl}-\hat{\sigma}_{lk}\delta_{mj} \tag{A3}$$

and application of the rotating-wave approximation. The resulting equations for the averaged atomic operators are

$$\frac{\partial}{\partial t}s_{11}=\frac{i}{2}(\Omega_P^*s_{12}-\Omega_Ps_{21})+A_{21}s_{22}\ , \tag{A4a}$$

$$\frac{\partial}{\partial t}s_{22}=\frac{i}{2}(\Omega_Ps_{21}-\Omega_P^*s_{12}+\Omega_Ss_{23}-\Omega_S^*s_{32})-(A_{21}+A_{23})s_{22}\ , \tag{A4b}$$

$$\frac{\partial}{\partial t}s_{33}=\frac{i}{2}(\Omega_S^*s_{32}-\Omega_Ss_{23})+A_{23}s_{22}\ , \tag{A4c}$$

$$\frac{\partial}{\partial t}s_{21}=-(\beta_{21}-i\Delta_P)s_{21}-\frac{i}{2}[\Omega_P^*(s_{11}-s_{22})+\Omega_S^*s_{31}]\ , \tag{A4d}$$

$$\frac{\partial}{\partial t}s_{32}=-(\beta_{32}+i\Delta_S)s_{32}-\frac{i}{2}[\Omega_S(s_{22}-s_{33})-\Omega_Ps_{31}]\ , \tag{A4e}$$

$$\frac{\partial}{\partial t}s_{31}=-[\beta_{31}+i(\Delta_S-\Delta_P)]s_{31}-\frac{i}{2}(\Omega_Ss_{21}-\Omega_P^*s_{32})\ , \tag{A4f}$$

$$\frac{\partial}{\partial t}s_{jk}=\frac{\partial}{\partial t}s_{kj}^*\ , \tag{A4g}$$

where the Stokes Rabi frequency is defined as

$$\Omega_S\equiv\frac{2}{\hbar}\mathbf{d}_{23}\cdot\mathbf{e}_S\mathcal{E}_S \tag{A5}$$

and the definitions of the other variables and parameters can be found in Sec. II.

Propagation of the electric field is described by the one-dimensional Maxwell equation

$$\left[\frac{\partial^2}{\partial z^2}-\frac{1}{c^2}\frac{\partial^2}{\partial t^2}\right]\mathbf{E}(z,t)=\frac{1}{\epsilon c^2}\frac{\partial^2}{\partial t^2}\mathbf{P}(z,t)\ , \tag{A6}$$

where $\mathbf{P}(z,t)$ is the polarization in the medium. The atomic polarization is given by

$$\mathbf{P}=N\langle\mathbf{d}\rangle_\Delta\ , \tag{A7}$$

where $\mathbf{d}=\langle\hat{\mathbf{d}}\rangle$ is the quantum-mechanical expectation value of the dipole moment operator:

$$\hat{\mathbf{d}}=d_{12}\hat{\sigma}_{12}+\mathbf{d}_{23}\hat{\sigma}_{23}+\text{H.c.}\ , \tag{A8}$$

and $\langle\ \rangle_\Delta$ indicates an averaging over detunings. The Doppler weighting is described by the line shapes

$$g_{21}(\Delta_{21}) = g_{21}(\Delta_P - \Delta_P^0) = \frac{T_{21}^*}{\pi} \exp\left[-\frac{[(\Delta_P - \Delta_P^0)T_{21}^*]^2}{\pi} \right], \quad \text{(A9a)}$$

$$g_{23}(\Delta_{23}) = g_{23}(\Delta_S - \Delta_S^0) = \frac{T_{23}^*}{\pi} \exp\left[-\frac{[(\Delta_S - \Delta_S^0)T_{23}^*]^2}{\pi} \right], \quad \text{(A9b)}$$

where $T_{jk}^* = \pi g_{jk}(0)$ is the inhomogeneous lifetime of the j-k transition and the Doppler detunings are measured from line center:

$$\Delta_P^0 = \omega_{21}^0 - \omega_P , \quad \text{(A10a)}$$

$$\Delta_S^0 = \omega_{23}^0 - \omega_S . \quad \text{(A10b)}$$

ω_{21}^0 and ω_{23}^0 are the transition frequencies of the stationary atom. The inhomogeneous lifetime T_2^* is related to the Doppler width [half width at half maximum (HWHM)], Δ_D by $T_2^* \Delta_D = (\pi \ln 2)^{1/2}$.

The reduced Maxwell equations (2.11) are obtained by substituting the assumed forms of the electric field, Eqs. (2.2a) and (2.4), into Eq. (A6) and employing the slowly-varying-envelope approximation.

APPENDIX B: THE THALLIUM ATOM

Raymer and Carlsten used atomic thallium in their investigations of SRS and stimulated collision-induced fluorescence.[13–16] We have chosen to use this atom to provide physical parameters for our numerical simulations. Due to level degeneracies the atom cannot be described by a simple three-state model. However, if we take both the pump and Stokes light to be linearly polarized, we can concern ourselves only with $\Delta m_j = 0$ transitions. These transitions are shown in Fig. 12. It is then easy to show that the definition of the Rabi frequency is independent of the initial spin of the electron since the electron-spin states do not mix. The atom then can be accurately modeled by three (nondegenerate) states in this case. The physical parameters which describe the thallium atom are taken from Ref. 36. They are $\omega_{21} = 4.99 \times 10^{15}$, $\omega_{23} = 3.51 \times 10^{15}$, $A_{21} = 6.25 \times 10^7$, and $A_{23} = 7.05 \times 10^7$, in units of rad/s.

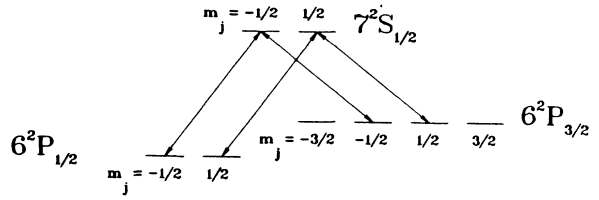

FIG. 12. Electronic transitions of atomic thallium used in the experiments in Refs. 13–16. Arrows show allowed dipole transitions for linearly polarized pump and Stokes light.

*Present address: Lockheed Palo Alto Research Laboratory, 3251 Hanover Street, Palo Alto, CA 94304.
†Also at the Institute of Optics, University of Rochester, Rochester, NY 14627.
‡Present address: Department of Physics, University of Oregon, Eugene, OR 97403.

[1]M. J. Konopnicki and J. H. Eberly, Phys. Rev. A **24**, 2567 (1981).
[2]K. J. Drühl, J. L. Carlsten, and R. G. Wenzel, J. Stat. Phys. **39**, 615 (1985); **39**, 621 (1985).
[3]R. L. Carman, F. Shimizu, C. S. Wang, and N. Bloembergen, Phys. Rev. A **2**, 60 (1970).
[4]M. G. Raymer, J. Mostowski, and J. L. Carlsten, Phys. Rev. A **19**, 2304 (1979).
[5]J. Mostowski and M. G. Raymer, Opt. Commun. **30**, 237 (1981).
[6]B. J. Herman, P. D. Drummond, J. H. Eberly, and B. Sobolewska, Phys. Rev. A **30**, 1910 (1984).
[7]C. M. Bowden and C. C. Sung, Phys. Rev. Lett. **50**, 156 (1983).
[8]T. A. De Temple, L. A. Bahler, and J. Osmundsen, Phys. Rev. A **12**, 2514 (1975).
[9]D. L. Rousseau, A. D. Patterson, and P. F. Williams, Phys. Rev. Lett. **34**, 1306 (1975).
[10]J. J. Wynne and P. P. Sorokin, J. Phys. B **8**, L37 (1975).
[11]J. L. Carlsten and P. C. Dunn, Opt. Commun. **14**, 8 (1975).
[12]E. Courtens and A. Szöke, Phys. Rev. A **15**, 1588 (1977); **17**, 2119 (1978).
[13]M. G. Raymer and J. L. Carlsten, Phys. Rev. Lett. **39**, 1326 (1977).
[14]J. L. Carlsten and M. G. Raymer, in *Laser Spectroscopy III*, edited by J. L. Hall and J. L. Carlsten (Springer-Verlag, New York, 1977), p. 205.
[15]M. G. Raymer, J. L. Carlsten, and G. Pichler, J. Phys. B **12**, L119 (1979).
[16]M. G. Raymer, Ph.D. thesis, University of Colorado, 1979 (unpublished).
[17]A. Crubellier, S. Liberman, D. Mayou, and P. Pillet, Opt. Lett. **8**, 105 (1983).
[18]Y. R. Shen, Phys. Rev. B **9**, 622 (1974).
[19]L. Allen and J. H. Eberly, *Optical Resonance and Two-Level Atoms* (Wiley, New York, 1975).
[20]B. J. Herman and J. H. Eberly, Opt. Commun. **62**, 130 (1987).
[21]M. D. Crisp, Phys. Rev. A **8**, 2129 (1973).
[22]P. W. Milonni and J. H. Eberly, J. Chem. Phys. **68**, 1602 (1978).
[23]B. R. Mollow, Phys. Rev. A **8**, 1949 (1973).
[24]See D. Grischowsky, Phys. Rev. A **14**, 802 (1976), and references therein.
[25]S. L. McCall and E. L. Hahn, Phys. Rev. **183**, 457 (1969).
[26]M. Takatsuji, Phys. Rev. A **4**, 808 (1971).
[27]N. Tan-no, T. Shirhata, K. Yokoto, and H. Inaba, Phys. Rev. **47A**, 241 (1974).
[28]N. Tan-no, T. Shirhata, K. Yokoto, and H. Inaba, Phys. Rev. A **12**, 159 (1975).
[29]D. Grischowsky, M. M. T. Loy, and P. F. Liao, Phys. Rev. A **17**, 2514 (1975).
[30]G. I. Kachen and W. H. Lowdermilk, Phys. Rev. A **14**, 1472 (1976).

[31]V. A. Gorbunov, Kvant. Elektron. (Moscow) **9**, 152 (1982) [Sov. J. Quantum Electron. **12**, 98 (1982)].
[32]J. N. Elgin and T. B. O'Hare, J. Phys. B **12**, 159 (1979).
[33]B. J. Herman, J. H. Eberly, M. G. Raymer, and J. L. Carlsten (unpublished).
[34]D. C. Burnham and R. Y. Chiao, Phys. Rev. **188**, 667 (1969).
[35]D. Mihalas, *Stellar Atmospheres*, 2nd ed. (Freeman, San Francisco, 1978), p. 279.
[36]A. Gallagher and A. Lurio, Phys. Rev. **A136**, 87 (1964).